TRI-PP--89-64

Search for mixing of muonium (μ^+e^-) and antimuonium (μ^-e^+)

T.M. Huber,[a] [*] G.A. Beer,[b] T. Bowen,[c] C.A. Fry,[d] [*] P.G. Halverson,[c] B. Heinrich,[e]

A.C. Janissen,[b] [+] K.R. Kendall,[e] A.R. Kunselman,[a] G.M. Marshall,[f] G.R. Mason,[b]

K. Myrtle,[e] A. Olin,[b] [+] J.B. Warren[g]

[a] University of Wyoming, Laramie, Wyoming 82071

[b] University of Victoria, Victoria, British Columbia, Canada V8W 2Y2

[c] University of Arizona, Tucson, Arizona 85721

[d] University of Rochester, Rochester, New York 14627

[e] Simon Fraser University, Burnaby, British Columbia, Canada V5A 1S6

[f] TRIUMF, Vancouver, British Columbia, Canada V6T 2A3

[g] University of British Columbia, Vancouver, British Columbia, Canada V6T 1W5

A search is described for mixing muonium (μ^+e^-) and antimuonium (μ^-e^+). Thermal muonium was produced by stopping muons in a SiO_2 powder target. As a conversion signature, a μ^- from antimuonium would create ^{184}Ta in an adjacent tungsten foil. The surface layer of the sample was chemically extracted and counted in a low-background germanium spectrometer; no conversion events were observed. The resulting upper limit on the probability that a muonium atom spontaneously converts to antimuonium is 2.0×10^{-6} (90% confidence). This corresponds to a limit of $0.28\ G_F$ on the effective four-fermion coupling constant between muonium and antimuonium.

PACS numbers: 13.35.+s, 14.60.Ef, 36.10.Dr

(submitted to Physical Review C)

I. INTRODUCTION

The standard model of electro-weak interactions[1] is a major triumph of theoretical physics. The model, however, contains some rather unnatural assumptions and numerous parameters. In recent years, extensions have been proposed which reduce the number of free parameters or eliminate some *ad hoc* assumptions of the standard model. The observation of a reaction, such as the mixing of muonium (μ^+e^- or Mu) and antimuonium (μ^-e^+ or $\overline{\text{Mu}}$), which is not allowed in the standard model, could test some of these theories. If a coupling exists between these states, a Mu atom can spontaneously convert to $\overline{\text{Mu}}$.

The first experimental search for Mu–$\overline{\text{Mu}}$ conversion, in 1968, placed a 95% confidence upper limit[2] of $G < 5800$ G_F on the four-fermion muonium–antimuonium coupling constant (where G_F is the Fermi coupling constant). A number of experiments[3,4] have placed more stringent upper limits on this conversion. The first run of the current TRIUMF experiment published the limit[5] $G < 0.88$ G_F (90% confidence) which was the first measurement below the weak interaction level. A preliminary upper limit of $G < 0.5$ G_F (90% confidence) has been quoted by a LAMPF experiment.[6] We report the final results of the TRIUMF experiment searching for conversion of muonium to antimuonium.

A. Theory

To explain the absence of rare muon decays, e.g. $\mu \rightarrow e\gamma$, $\mu \rightarrow 3e$, and muonium–antimuonium conversion, several lepton number conservation rules have been suggested. These include an additive law[7] and a multiplicative, parity–like law for muon number conservation.[8] The lepton generation numbers can be assigned as $L_\ell = +1$ for the leptons ℓ^- and ν_ℓ, $L_\ell = -1$ for the leptons ℓ^+ and $\overline{\nu_\ell}$, where ℓ indicates e, μ, or τ. The multiplicative law requires that the total lepton number is conserved [$\sum(L_e + L_\mu + L_\tau) = $ const.] and also the muon number parity $(-1)^{\sum L_\mu}$ is conserved. This multiplicative law prohibits reactions such as $\mu \rightarrow e\gamma$, $\mu \rightarrow 3e$, and $\mu(Z, A) \rightarrow e(Z, A)$, however it allows muonium–antimuonium conversion $(\mu^+e^- \rightarrow \mu^-e^+)$ and muon decay with "wrong" neutrinos $(\mu^+ \rightarrow e^+\overline{\nu_e}\nu_\mu)$. The more restrictive additive law requires that each lepton generation number is separately conserved $(\sum L_\ell = $ const.); this law prohibits the same decays as the multiplicative law, while also prohibiting Mu–$\overline{\text{Mu}}$ conversion and "wrong" neutrino muon decay. The absence of observation of muon decay with "wrong" neutrinos[9] has led to the general adoption of the additive law. In many extensions to the standard model, however, lepton number conservation is not an exact symmetry, thus reactions which do not conserve lepton number will occur. Within these models, speculation on the values of relevant parameters allows estimation of limits on the rates of rare decay processes.

In discussing various lepton number conservation schemes, Pontecorvo[10] in 1957 suggested that Mu may be able to spontaneously convert to $\overline{\text{Mu}}$. In 1961, Feinberg and Weinberg[11] worked out the detailed phenomenology of Mu–$\overline{\text{Mu}}$ conversion. They expressed the interaction in terms of a four fermion V–A interaction which does not conserve lepton number:

$$\mathcal{H} = \frac{G}{\sqrt{2}}\overline{\psi}_\mu\gamma_\lambda(1 - \gamma_5)\psi_e\overline{\psi}_\mu\gamma^\lambda(1 - \gamma_5)\psi_e + \text{H.c.,} \tag{1}$$

where G is the effective coupling strength. The resulting matrix element is

$$\langle\overline{\text{Mu}}\,|\mathcal{H}|\text{Mu}\rangle = \delta/2 = 1.0\times10^{-12}(G/G_F)\quad\text{eV.} \tag{2}$$

In the absence of magnetic fields, Mu and $\overline{\text{Mu}}$ atoms have the same energy E_0 in the electromagnetic Hamiltonian $\mathcal{H}_0$. The eigenstates of the combined Hamiltonian $\mathcal{H} + \mathcal{H}_0$ are $(|\text{Mu}\rangle \pm |\overline{\text{Mu}}\rangle)/\sqrt{2}$ with energies $E_0 \pm \delta/2$. Since Mu and $\overline{\text{Mu}}$ are not eigenstates of the combined Hamiltonian, a Mu atom can convert to $\overline{\text{Mu}}$ in much the same way that a K^0 beam develops a component of $\overline{K^0}$. Within this framework, Feinberg and Weinberg calculated the probability that a Mu atom will convert to $\overline{\text{Mu}}$ before decaying:

$$P(\overline{\text{Mu}}) = \frac{\delta^2}{2\hbar^2\lambda^2} = C\left(\frac{G}{G_F}\right)^2, \tag{3}$$

where λ is the muon decay rate, and $C = 2.5\times10^{-5}$ is the probability of a Mu-$\overline{\text{Mu}}$ conversion at a coupling strength of $G = G_F$. The probability that a Mu atom created at $t = 0$ is identified as $\overline{\text{Mu}}$ at time t is given by

$$P(t) = \sin^2\left(\frac{\delta t}{2\hbar}\right)e^{-\lambda t} \approx C\left(\frac{G}{G_F}\right)^2 \frac{(\lambda t)^2}{2}e^{-\lambda t}, \tag{4}$$

which has a maximum probability at $t = 2/\lambda$.

In a magnetic field H, the degeneracy of the $(F, m_f) = (1, \pm1)$ Mu and $\overline{\text{Mu}}$ states is broken by a Zeeman splitting[11] $\Delta = 2\mu_B H$ (where F is the total spin and μ_B is the Bohr magneton). If the splitting Δ is larger than $\hbar\lambda$ (or $H \gtrsim 25$ mG), these two states will not mix during the muon lifetime. Since half the muonium atoms will be in the $(F, m_f) = (1, \pm1)$ states, the probability of Mu-$\overline{\text{Mu}}$ conversion will be reduced by a factor of two for fields larger than 25 mG.

In the standard model, neutrinos and antineutrinos are distinct (referred to as Dirac neutrinos), however in many extensions of the standard model neutrinos may have a Majorana component (neutrino=antineutrino). Several of these models (e.g. left-right symmetric[12] and supersymmetric[13] models) use a "see-saw" mechanism[14] to explain the observation of "light" left-handed neutrinos ($m_\nu \lesssim 1$ eV/c^2) and "heavy" (thus far unobserved) right-handed neutrinos ($M_\nu \gtrsim 50$ GeV/c^2). Muonium-antimuonium conversion can occur directly by Majorana neutrino exchange[15]; however the coupling is second order and has been estimated to be $G \lesssim 3\times10^{-6}$ G_F.

Left-right symmetric models conserve parity and charge conjugation before spontaneous symmetry breaking. In addition to the doublet of Higgs bosons of the standard model, this model postulates the existence of an additional Higgs triplet $(\Delta^0, \Delta^+, \Delta^{++})$. Majorana neutrino masses are generated by the neutral member Δ^0 of the Higgs triplet, and muonium conversion can occur via the exchange of a doubly charged Higgs boson Δ^{++} [e.g. Fig. 1(a)]. The Hamiltonian for Mu to $\overline{\text{Mu}}$ conversion[16,17] via this process is

$$\mathcal{H}_{++} = \frac{f_{ee}f_{\mu\mu}^*}{4M_{++}^2}\,\overline{\psi_e^c}(1 - \gamma_5)\psi_e\overline{\psi}_\mu(1 + \gamma_5)\psi_\mu^c + \text{H.c.} \tag{5}$$

where f_{ee} and $f_{\mu\mu}$ are couplings of electrons and muons to the doubly charged Higgs boson Δ^{++} with mass M_{++}. It is possible, using the Fierz transform, to rewrite this expression in the form of Eq. (1); equating the coupling constants gives[17]

$$\frac{G}{G_F} = \frac{f_{ee}f_{\mu\mu}^*}{g^2}\left(\frac{M_W}{M_{++}}\right)^2 \tag{6}$$

where M_W is the W boson mass and $g^2 = 8G_F M_W^2 / \sqrt{2}$ is the dimensionless coupling constant of the standard model. Using suitable estimates for f_{ee} and $f_{\mu\mu}^*$, one can extract a lower limit on the mass of the doubly charged Higgs.

The conversion of muonium to antimuonium may not be constrained by other rare decay experiments. Within the left–right symmetric model, neutrinoless double beta decay can occur by emitting a doubly charged Higgs[18] as illustrated in Fig. 1(b). This decay is strongly suppressed by two couplings of a normal Higgs (ϕ^-) or right handed W bosons.[19] Other rare decays such as $\mu \rightarrow e\gamma$, $\mu \rightarrow 3e$, $K^0 \rightarrow \mu e$, and $\mu(Z, A) \rightarrow e(Z, A)$ do not constrain the model in the same way as Mu to $\overline{\mathrm{Mu}}$. These decays involve μ–e couplings, and there is no inherent reason to believe μ–e couplings have the same strength as μ–μ and e–e couplings.

Within the Gelmini–Roncadelli[20] model (which incorporates a doubly charged Higgs boson), Halprin[15] estimated the Mu–$\overline{\mathrm{Mu}}$ coupling strength could be as large as $10\ G_F$. This model, however, is strongly constrained by other rare decay experiments[21] because it assumes $f_{e\mu} = f_{ee} = f_{\mu\mu}$; recent estimates on Mu–$\overline{\mathrm{Mu}}$ conversion in this model[16,22] are $G \lesssim 10^{-9}\ G_F$. Muonium conversion to antimuonium has been discussed in the context of other models,[22,23] however with vanishingly small coupling constants of $G \ll 10^{-10}\ G_F$.

B. Overview of the experiment

In our experiment, muonium was formed[4] by stopping a μ^+ beam in a finely divided fused SiO_2 powder target in the apparatus of Fig. 2. Mu atoms diffused out of the powder into the vacuum where conversion of Mu to $\overline{\mathrm{Mu}}$ could take place. At the adjacent tungsten oxide catcher surface, the μ^- (from $\overline{\mathrm{Mu}}$) could undergo atomic and nuclear capture on W producing $^{184}\mathrm{Ta}$. Detection of nuclear activation would signify that a Mu atom had converted to $\overline{\mathrm{Mu}}$ before reaching this foil. After each twelve hour exposure to μ^+ (henceforth referred to as a "$\overline{\mathrm{Mu}}$ exposure"), a thin layer was chemically removed from the W foil and was counted in the shielded low level counting (LLC) apparatus (Fig. 3). $^{184}\mathrm{Ta}$ nuclei decay with an 8.7 h half-life by β emission to excited states of $^{184}\mathrm{W}$ with a distinctive decay signature (Fig. 4). This radio-chemical detection technique for antimuonium has a relatively high efficiency coupled with a very low background.

In the following section, details of the apparatus are given. Section III describes the exposure and counting cycles. In Sec. IV the detection efficiency for antimuonium is calculated. The experimental results are given in Sec. V.

II. APPARATUS

A. $\overline{\mathrm{Mu}}$ exposure apparatus

The experiment was performed on the M15 beamline[24] at TRIUMF. Because this channel has two bends in two different planes and an electrostatic separator, the muon beam is quite free of contamination from both neutral (neutrons and photons) and charged (pions and electrons) particles. For a 500 MeV 150 μA proton beam incident on a carbon production target, this beamline delivered a flux of 1.3×10^6 μ^+/s at 28.5 MeV/c with a 10% momentum spread. By reversing the polarity of the beamline magnets, a negative muon flux of 5500 μ^-/s (at 28.5 MeV/c) was obtained.

The apparatus used for $\overline{\mathrm{Mu}}$ exposures, which attached to the M15 beamline, is shown in Fig. 2. The isolation valve divided the vacuum system into two separate chambers: the antechamber, where the W foil was introduced and cleaned, and the

ultra high vacuum (UHV) chamber (containing the SiO$_2$ muonium production target) which was kept under vacuum. The majority of the vacuum system was made of 10 cm (inside diameter) stainless steel tube, with attached ports holding gauge heads, roughing lines, and a high voltage feedthrough. At the upstream end of the UHV chamber was the target cube (15 cm across), which surrounded the SiO$_2$ powder target. The vacuum pumps were an ion pump in the UHV chamber and cryopumps in the UHV chamber and antechamber. Pressures were measured by thermocouple, Pirani and ionization gauges; a residual gas analyzer determined the gas composition in the vacuum system. The antechamber could be filled with O$_2$ for oxygen plasma cleaning, or N$_2$ for venting the system.

Muons entered through a 25 μm stainless steel window which separated the UHV chamber from the beamline vacuum. The incident muon beam was measured by a 3.5 cm diameter disk of 0.25 mm NE102 plastic scintillator mounted upstream of the target cube. Positron contamination in the incident beam could be determined by the pulse height in this beam scintillator.

The Mu production target was Cab-O-Sil EH-5 grade SiO$_2$ powder (7 nm average diameter)[25] with thickness of 22 mg/cm^2 along the beam direction. The powder was supported by a 0.12 mm thickness Al foil tray with a 66° angle between the beam and the normal to the powder (Fig. 5). Since the UHV chamber was kept evacuated during W foil changes, each powder target was used for many $\overline{\text{Mu}}$ exposures.

To indicate muonium–antimuonium conversion, $\overline{\text{Mu}}$ atoms would create ^{184}Ta atoms at the surface of the catcher foil, an 8 cm by 11 cm piece of 25 μm tungsten foil bent to have 1.8 cm "wings" at 45° (Fig. 6). The catcher foil was supported parallel to the SiO$_2$ target by a frame attached to a sliding support structure. A positioning ring and locking mechanism located the support within the target cube such that the distance between the catcher foil and SiO$_2$ powder was 1.8 ± 0.2 cm. To insert and retrieve the catcher support, a 1.5 cm diameter "catcher rod" (which entered the vacuum chamber through a small, differentially pumped volume sealed by two viton O-rings) could be moved the length of the vacuum system. To axially align the catcher rod, three stainless steel braces attached to the rod slid along the inside of the vacuum tube. The catcher rod screwed into a nut attached to the catcher support, so the rod could be withdrawn when the catcher support was locked in place in the target cube.

Since magnetic fields larger than 25 mG would suppress the Mu to $\overline{\text{Mu}}$ conversions, the target region was surrounded by three separate layers of passive magnetic shielding (Fig. 2). Inside the vacuum system was a cylindrical shield of 0.7 mm Conetic high magnetic susceptibility shielding. Although the position resolution was somewhat degraded, it was possible to perform muonium yield measurements without removing this inner shield. A box of 1.6 mm thickness Conetic shielding, which fit around the outside of the target cube, was removable to permit yield measurements. The outer layer of shielding was a 5 cm thick iron yoke which surrounded the front, back, top and bottom of the target cube. The shielding was systematically degaussed by passing a 60 Hz alternating current through coils fitted to this yoke. To demonstrate the effectiveness of the shielding, the residual field was measured with a saturable inductor magnetometer probe inserted into the target cube.

Muonium yields were measured by observing the μ^+ decay positrons which exited through a 10 cm diameter, 25 μm stainless steel window on the target cube. A telescope consisting of three multi-wire proportional chambers, scintillators and a large NaI(Tl) detector determined the trajectory and energy of decay positron, as well as the decay time. Details of this apparatus are discussed in Refs. 4 and 26.

B. Low level counting apparatus

Activity in a sample was measured in the low level counting (LLC) apparatus (Fig. 3) which was located in a separate building from the beamline and cyclotron. To detect the characteristic signature of ^{184}Ta (Fig. 4), the LLC apparatus consisted of two plastic scintillators in front of two Ge detectors. Concentric cylinders of 3.7 cm thickness copper and tungsten shielded the detection system. The two halves of the system were mounted independently so the shielding and detectors could be separated to permit insertion of the sample. Three cosmic ray veto scintillators (31 × 17 × 1 cm^3) were supported above the shielding, and two additional veto scintillators were placed on the sides.

Decay γ's were measured by n-type intrinsic Ge detectors with volumes of 87.1 cm^3 and 86.0 cm^3. A pileup occurred when the delay between two γ's in the same detector was $\lesssim 4$ μs, because the Ge detector amplifier would integrate the total energy of both pulses. If the second γ in the same detector was delayed by > 4 μs, the first γ's energy [E(prompt)] could be measured along with the second γ's delay time [t(delay)]. When the delayed γ was in the opposite detector as the prompt γ, we could measure both the prompt [E(prompt)] and delayed [E(delay)] γ energies in addition to the delayed γ time [t(delay)].

The plastic scintillators, for detecting decay β's, were 3.2 cm diameter discs of 3.5 mm thickness NE102. Each scintillator was joined to a light guide shaped to pass through the shielding to a photomultiplier tube. To minimize β energy losses, a single thickness of 25 μm aluminized mylar wrapped the scintillator.

For the LLC electronics, the 25 μs event gate was started by either of the two Ge detectors. Each Ge detector, β scintillator and veto counter had a short range (0–100 ns) time to digital converter (TDC) to measure prompt coincidences between detectors along with a long range (0–25 μs) TDC to measure delayed detector events. CAMAC scalers recorded the number of times that each detector was triggered. A tape record was written which included the TDC values, and the energies of both Ge detectors and β scintillators. A 350 μs computer–busy gate allowed time to record the event; for each run, the live-time fraction was determined by counting the number of computer–busy gates in coincidence with a 10 Hz pulser.

III. MUONIUM CONVERSION EXPERIMENT

A. Exposure cycle

The search for Mu–$\overline{\text{Mu}}$ conversion was done during twelve hour "$\overline{\text{Mu}}$ exposure" cycles. To begin this cycle, with the isolation valve closed and the antechamber vented, a W foil was attached to the catcher support in the antechamber. Next, the antechamber was sealed and pumped to about 10^{-6} Torr.

To remove the hydrocarbons which covered the foil, and to oxidize the W surface, an oxygen plasma[27] was used. The discharge, in 50 mTorr of oxygen, was formed by a 1000V 150 mA ion pump power supply attached to a high voltage feedthrough. A bluish–white plasma filled the antechamber when the O$_2$ pressure was adjusted correctly. After a two minute cleaning, the cryopump valve was opened. When the antechamber pressure reached 10^{-6} Torr, about one minute after the plasma cleaning ended, the catcher was moved into the UHV chamber. After locking the catcher support in place, the catcher rod was retracted, the isolation valve was closed and the muon beam was turned on. The UHV chamber pressure dropped to $< 10^{-7}$ Torr a few seconds after closing the isolation valve, and slowly went to 1×10^{-8} Torr over the 10 h run. The integrated vacuum exposure during a $\overline{\text{Mu}}$ exposure was $\sim 2.2 \times 10^{-3}$ Torr s.

At the end of each $\overline{\text{Mu}}$ exposure, the muon beam was turned off, and the

catcher support (with the exposed W foil) was moved from the UHV chamber to the antechamber using the catcher rod. After venting the antechamber, the exposed W foil was removed and processed (see following section), another foil was inserted, and the $\overline{Mu}$ exposure cycle was repeated. The elapsed time between the end of one exposure and the beginning of the next run was about 40 min.

B. Counting cycle

In parallel with the exposure cycle outlined above, the residue from previous exposures was counted in the LLC apparatus. The chemical processing and counting cycle for a $\overline{Mu}$ exposure is now described.

As discussed in Sec. IV E below, any ^{184}Ta formed during a $\overline{Mu}$ exposure would be deposited be within 28 nm of the surface of the W foil. To strip off the surface, the anodization process[28] was used: The W foil was attached to the anode of a 70 V power supply and immersed in an aqueous solution of 0.4 M KNO_3 and 0.04 M HNO_3. Within one minute, 70 $\mu g/cm^2$ (36 nm) of both sides of the foil was oxidized into WO_3. The WO_3 was then dissolved in a 15% solution of NH_4OH in distilled water; any ^{184}Ta in the anodized layer would remain in this solution. The anodization and dissolving procedure were repeated to strip another 36 nm of the W surface into the same solution. The W foil was weighed before and after stripping to determine the amount of W removed.

To condense the ^{184}Ta in the NH_4OH solution to a small sample, the solution was carefully boiled in an Erlenmeyer flask until only a few mℓ containing the residue remained. This was poured into a dish shaped from a 4 cm piece of 10 μm Al foil. The glassware was rinsed with another 10 mℓ of NH_4OH which was poured into the Al foil. After gently heating the foil until all the solution evaporated, the residue was held in place by folding the Al foil in half. The entire chemical extraction process took between one and two hours. The Al foil containing the ^{184}Ta residue was counted for about 10 h in the LLC apparatus, until the next $\overline{Mu}$ exposure was ready to be counted.

In alternate exposures, the counting time in the LLC apparatus was doubled by re-using the Al foil. After unfolding the Al foil from the first exposure, the few mℓ of NH_4OH solution containing ^{184}Ta from the second exposure was added to the precipitate from the first exposure. The liquid was evaporated, leaving the residue from both exposures in this foil.

C. Determination of muon flux

To determine the muon flux, pulses from the thin beam scintillator were mea-sure. Figure 7 shows the pulse height spectrum observed in this scintillator during a μ^+ t. The peak below channel 150 corresponds to a positron contamination of $(11 \pm 1)\%$ which come principally from μ^+decays in the target. After subtracting the positron contamination, the total μ^+ flux was $N_\mu = (2.3 \pm 0.2) \times 10^{12}$ during the 525 h devoted to searching for Mu conversion to $\overline{Mu}$.

D. Analysis of low level counting data

Off-line analysis selected LLC events which met various criteria. Events were rejected if one of the veto scintillators fired in coincidence with the prompt γ. An event was classified as a β-γ event if the β time (measured by the short range TDC) was within 30 ns of the prompt γ, and the β pulse height was larger than the noise threshold. (The β scintillator noise threshold was the pulse height measured when the scintillator was not in coincidence with a γ.) For an event to qualify as a γ-γ_{del} event, none of the veto counters could have been triggered within 400 ns of the delayed γ,

and the delayed gamma time t(delay) was either: (a) in the interval $4 < t$(delay) $<$ 25 μs if the delayed γ was in the same detector as the prompt γ, or (b) in the interval $0.15 < t$(delay) < 25 μs if the delayed γ was in opposite detector as prompt the γ. A β-γ-γ_{del} event satisfied the criteria of both a β-γ and γ-γ_{del} event.

The major γ-γ_{del} background observed in the LLC apparatus was due to a metastable state of ^{72}Ge. The 691 keV 0^+ first excited state of ^{72}Ge has a 439 ± 4 ns half-life and emits a 691 keV γ when it decays.[29] This state is excited by reactions such as ^{72}Ge(n,n$'\gamma$)^{72}Ge, and is commonly observed in γ spectra taken with Ge detectors. Figure 8 shows the delayed γ energy distribution for all γ-γ_{del} events recorded during the 602 h counting of the $\overline{\text{Mu}}$ exposures. The peak observed for E(delay)=700 ± 10 keV contains approximately 6% of the total γ-γ_{del} events. Figure 9 shows the time distribution of the γ-γ_{del} events with E(delay) between 690 and 710 keV, consistent with the 439 ns half-life of ^{72}Ge.

IV. EXPERIMENTAL EFFICIENCY

A. Overview of experimental efficiency

In this section, measurement of the efficiency of the experiment is discussed. The detection efficiency per incident muon is given by

$$\epsilon_\mu = Y \cdot e \cdot f \cdot g \cdot h, \tag{7}$$

where the factors e, f, and g are defined in the following paragraphs. The yield Y of thermal muonium in vacuum per incident muon is discussed in Sec. IV D, and Sec. IV B describes the time correction h due to the finite exposure and counting times for ^{184}Ta. Table I lists the value of all factors in the efficiency ϵ_μ. For N_μ incident muons, the number of expected antimuonium events was $N = P(\overline{\text{Mu}})S$, where $P(\overline{\text{Mu}})$ is the probability that Mu can convert to $\overline{\text{Mu}}$, and $S = N_\mu \epsilon_\mu$.

The catcher detection fraction e is a product of factors relating to the Mu–$\overline{\text{Mu}}$ detection efficiency of the catcher and its geometry

$$e = e(\text{field}) \cdot e(\text{catcher}) \cdot e(\text{surface}) \cdot e(\text{recoil}). \tag{8}$$

The factor e(field) is a small correction to the Mu to $\overline{\text{Mu}}$ conversion probability due to residual magnetic fields. The fraction of Mu which convert to $\overline{\text{Mu}}$ before striking the catcher surface is given by e(catcher). Contamination on the WO_3 surface is incorporated into the factor e(surface). When negative muons capture on W nuclei, the resulting ^{184}Ta ions recoil, and only a fraction e(recoil) remain in the surface of the catcher foil. The determination of these factors is discussed in Sec. IV E.

The ^{184}Ta production efficiency f is the product of the following factors

$$f = f(\text{capture}) \cdot f(\text{nuclear}) \cdot f(184) \cdot f(\text{chemistry}), \tag{9}$$

which are discussed in Sec. IV F. For $\overline{\text{Mu}}$ atoms arriving at the WO_3 catcher surface, the μ^- undergoes atomic and nuclear capture on W with respective probabilities f(capture) and f(nuclear). A fraction f(184) of nuclear μ^- captures would produce ^{184}Ta. The chemical extraction efficiency of ^{184}Ta from the W catcher surface is f(chemistry).

The combined efficiency for ^{184}Ta detection in the LLC apparatus is

$$g = g(\text{decay}) \cdot g(\beta) \cdot g(\gamma) \cdot g(\gamma_{\text{del}}) \cdot g(\text{pileup}). \tag{10}$$

The branching ratio $g(\text{decay})$ is the fraction of ^{184}Ta which decay emitting a β and 414 keV γ to a metastable ^{184}W state. The detection efficiencies in the LLC apparatus are $g(\beta)$ and $g(\gamma)$ for the decay beta and gamma. The apparatus detects a fraction $g(\gamma_{\text{del}})$ of delayed γ's from the cascade of the metastable state. The gamma detection efficiency will be reduced by $g(\text{pileup})$ due to delayed γ's which occur during the integration time of the Ge detector amplifier. Section IV G describes how g was determined.

B. ^{184}Ta lifetime corrections

The factor h contains corrections due to the ^{184}Ta lifetime. For a uniform production rate, the fraction of ^{184}Ta which does not decay during the beam exposure is $h(\text{beam}) = [1 - \exp(-\lambda t_b)]/\lambda t_b$, where t_b is the elapsed beam time and $\lambda = \ln 2/\tau$ is the decay rate for the $\tau = 8.7$ h half-life of ^{184}Ta. The fraction of ^{184}Ta which decays during counting in the LLC apparatus is $h(\text{LLC}) = [\exp(-\lambda t_i) - \exp(-\lambda t_f)]$, where t_i and t_f are starting and ending counting times (relative to the end of the exposure t_b) in the LLC apparatus.

The live-time correction $h(\text{live})$ was also determined for each run. While an event was being transfered to tape, a 350 μs computer–busy gate rejected later events. A total N_p counts from a 10 Hz pulser occurred during an LLC run, of which N_b of the pulser signals occurred during a computer–busy gate. The live-time fraction for each run was $h(\text{live}) = (N_p - N_b)/N_p$, which had a value of 0.98 ± 0.01 for the $\overline{\text{Mu}}$ exposures. Calculation of the time factor for $\overline{\text{Mu}}$ exposures gives $h = h(\text{beam})h(\text{LLC})h(\text{live}) = 0.56 \pm 0.02$.

C. Negative muon measurements

As a direct measurement of many of the factors in f and g, W samples were irradiated with μ^- and the resulting ^{184}Ta was counted in the LLC apparatus. The number of ^{184}Ta atoms in a W sample after exposure in a μ^- beam is:

$$N(\text{Ta}) = N_\mu \cdot f(\text{nuclear}) \cdot f(184) \cdot h(\text{beam}) \cdot D, \tag{11}$$

where D is the fraction of the μ^- beam which stopped within the sample. When the sample was counted in the LLC apparatus, the expression for the number of γ's with energy $E(\text{prompt})=414$ keV is:

$$N(414) = N(\text{Ta}) \cdot f(\text{chemistry}) \cdot g(\text{decay}) \cdot g(\gamma) \cdot g(\text{pileup}) \cdot h(\text{LLC}) \cdot h(\text{live}), \tag{12}$$

with a value of $f(\text{chemistry})=1$ when a sample was counted without chemical processing. The number of $E(\text{prompt})=414$ keV γ's in a run was determined by fitting the γ energy spectra (as in Fig. 10) to a Gaussian distribution plus linear background.

The μ^- stopping fraction D was determined for each sample. For in situ measurements with a SiO_2 target in place, the μ^+ momentum was adjusted so half the stops were in the catcher; switching the beamline polarity to μ^- and attaching a thick W sample to the catcher, a stopping fraction $D = 0.5$ was obtained. In other runs, the full μ^- beam was stopped in a stack of W foils placed directly on the beamline window, thus $D = 1$.

After each μ^- exposure, one W foil was stripped and the residue was counted in the LLC apparatus. In a vertical stack of 25 μm W foils, the μ^- stopping distribution is two foils wide. In a foil not containing the peak of the stopping distribution, the ^{184}Ta distribution was approximately linear with increasing distance in the foil. The stopping fraction in the residue stripped from both sides of the foil, $D(\text{residue})$,

as compared to the stopping fraction in the the full foil, $D(\text{foil})$, was estimated by comparing the mass m_f of the full foil to the foil after stripping m_s according to

$$D(\text{residue})/D(\text{foil}) = (m_f - m_s)/m_f. \qquad (13)$$

More sophisticated stopping power calculations in a Monte Carlo simulation predict essentially the same result.

D. Muonium yield

Previous experiments have shown that fine SiO_2 powder produces large amounts of thermal muonium in vacuum.[4,30] The muonium yield Y (per incident μ^+) in this experiment was measured by imaging the μ^+ decay positron with a wire chamber telescope (see details in Refs. 4 and 26). Projecting the positron trajectory to the center of the target cube gives the Mu decay position. The μ^+ decay time was plotted for 1 cm regions successively further from the target. Due to finite position resolution and parallax, the position of μ^+ decays in the target were sometimes extrapolated to the wrong spatial region, leading to a 2 μs muon decay background in regions distant from the target. In addition to the exponential background, a broad peak was observed in the time distributions for regions distant from the target. This peak, which was seen later in regions further from the target, is consistent with muonium drifting with thermal velocity from the target. The experimentally measured timing distributions were compared to a Monte Carlo simulation to determine the Mu yield.[4,26] This simulation modeled both the diffusion of muonium into the vacuum and the subsequent imaging of the decay positrons in the wire chamber telescope.

The maximum muonium yield in vacuum occurs when Mu was produced near the downstream surface of the SiO_2 powder. The peak of the μ^+ stopping distribution was positioned at the surface of the SiO_2 target by varying the μ^+ momentum until half the muon decays were in the powder and half continued through and stopped in the catcher. During the 50 $\overline{\text{Mu}}$ exposures, four different SiO_2 targets (roughly 22 mg/cm^2 normal to the beam direction) were used. The muonium yield (per incident muon) varied from 0.014 ± 0.003 to 0.026 ± 0.005, with an average yield of $Y = \sum_i (N_i Y_i)/N_\mu = 0.024 \pm 0.003$ where N_i and Y_i are the number of incident muons and yield, respectively, in exposure i.

E. Catcher detection fraction

If muonium conversion occurs, antimuonium would activate tungsten atoms in the catcher surface. The efficiency of the catcher geometry, along with other factors related to the catcher, are grouped in the catcher detection fraction ϵ.

With the beamline magnets on, the magnetic field in the muonium drift region was < 5 mG with gradients of less than 1 mG/cm. The reduction of the Mu–$\overline{\text{Mu}}$ conversion probability by this magnetic field[11] was less than 2%; thus $\epsilon(\text{field}) > 0.98$.

The Monte Carlo simulation was used to calculate the probability $\epsilon(\text{catcher})$ that a Mu atom would have converted to $\overline{\text{Mu}}$ and reached the catcher surface before decaying. For each simulated Mu atom, the program calculated the time between when the atom diffused out of the SiO_2 powder and when it struck the catcher (if it did not decay prior to reaching the catcher). Utilizing the time dependence of Eq. (4), the probability of a Mu–$\overline{\text{Mu}}$ conversion was calculated. For the catcher foil, shaped as in Fig. 6, positioned 1.8 ± 0.2 cm from the SiO_2 powder, the simulation indicates a value of $\epsilon(\text{catcher}) = 0.187 \pm 0.005$; less than a 10% variation is indicated for distances between 1.5 cm and 2.5 cm.

Calculations of antimuonium collisions with hydrogen and argon atoms[31] indicate that the inelastic cross section leading to atomic muon capture strongly domi-

nates competing processes. We expect this also to be true at the WO_3 surface, where the μ^- is strongly attracted and has a high transition rate to $\mu^- W$ atomic levels, while the positron will annihilate with an electron from the surface. Unfortunately an experiment to verify this requires a $\overline{Mu}$ beam and is thus not feasible.

A μ^- which captures on a molecule will tend to transfer to the atom with the largest nuclear charge Z, however it is not clear whether the μ^- would transfer from a contaminant on the surface to a W atom. To quantify the surface contamination, off-line experiments were performed using Auger electron spectroscopy (AES)[32] and x-ray photoelectron spectroscopy (XPS).[33] In these techniques, a beam (electrons in AES and x rays in XPS) ionizes an atom and causes it to emit an Auger electron or photoelectron. After oxygen plasma cleaning a W sample, the electron energy spectra were compared with reference spectra,[32,33] to obtain the following results: (a) at least seven monolayers of WO_3 covered the W foil, (b) small concentrations of potassium and calcium were observed, presumably chemically bonded to tungsten and thus of little concern, (c) the upper limit on the carbon contamination was 0.12 ± 0.03 monolayers, with no additional buildup on exposure to residual CO and CO_2 in the vacuum system, and (d) no evidence for H_2O contamination was observed. Thus, the fraction of surface free from contaminants was $e(\text{surface}) > 0.88 \pm 0.03$. Details of the surface tests are discussed in Appendix A.

The ^{184}Ta ions resulting from μ^- capture on a W atom would recoil with a maximum energy of 33 keV. Since $\overline{Mu}$ atoms would have captured at the surface, half of the recoils would be away from the substrate. With the winged catcher geometry used, calculations indicate 15% of the recoils out of the foil would strike the wings of the W foil. Therefore, a fraction $e(\text{recoil}) = 0.57 \pm 0.02$ of recoiling ^{184}Ta ions would remain in the foil. The measured 36 nm range[28] of 40 keV ^{133}Xe ions in W can be scaled to indicate a range of 28 nm for 33 keV ^{184}Ta ions in W. At least 72 nm of W was removed after each exposure, thus virtually all the ^{184}Ta ions which recoiled into the W substrate or were caught by the wings would be within the layer removed by the anodization procedure.

F. ^{184}Ta Production Fraction

To detect antimuonium, we searched for ^{184}Ta. The fraction f of $\overline{Mu}$ which would produce ^{184}Ta in the sample is now discussed.

The muonic capture ratio (the fraction of μ^- captured per W atom compared to an O atom) in WO_3 has been measured[34] to be $A(W/O) = 5.75 \pm 0.67$. This corresponds to $f(\text{capture}) = 0.67 \pm 0.03$ for the fraction of μ^- which capture on a W atom to the total number of stops. To confirm this value, in a separate experiment, a Ge detector was used to measure the atomic x rays from μ^- incident on W and WO_3 samples placed behind a Cu collimator in the beamline. The number of incident muons was determined both by beam scintillator pulses, and by Cu x rays observed. The resulting fraction, 0.6 ± 0.1, of μ^- which capture on W is consistent with the more accurate measurement of $f(\text{capture})$ listed above.

When a μ^- captures on a W atom, it would cascade to lower orbitals and capture on the nucleus. The measured 78.4 ± 1.5 ns lifetime[35] of μ^- in W implies that a fraction $f(\text{nuclear}) = 0.97 \pm 0.02$ will capture on the nucleus instead of decaying in orbit.

To form ^{184}Ta, a μ^- can capture either on ^{184}W and emit no neutrons or on ^{186}W and emit two neutrons. Equations (11) and (12) express the number of $E(\text{prompt}) = 414$ keV γ's observed when a W foil exposed to μ^- was counted in the LLC. The detection efficiencies $[g(\text{decay}) \cdot g(\gamma) \cdot g(\text{pileup})]$ were measured separately (Sec. IV G below), and the time correction h (Sec. IV B) was calculated for

each μ^- run. For N_μ incident muons with a known stopping distribution D (e.g. entire μ^- beam stopping in stack of foils, with a value of $D = 1$) the only factor in Eq. (12) not directly measured is $f(184)$. Averaging several μ^- runs results in $f(184)$=0.107 ± 0.003. This measurement of $f(184)$ is directly related to the efficiency of ^{184}Ta detection, thus it incorporates the uncertainties in the other factors used for the calculation.

As a check of this value of $f(184)$, the zero and two neutron emission probabilities for μ^- captures on lead were used. The isotopic abundances[36] are 30.7% for ^{184}W and 28.7% for ^{186}W. The zero and two neutron emission probabilities for ^{206}Pb and ^{208}Pb after μ^- capture[37] are 0.324 ± 0.022 and 0.137 ± 0.018 respectively, giving an estimate of 0.14 ± 0.01 for $f(184)$. The value of $f(184)$ directly measured by μ^- exposures is slightly smaller than this estimate based on neutron emission probabilities of lead.

f(chemistry) is the efficiency of the stripping procedure for removal of ^{184}Ta from the surface of a W foil. To measure f(chemistry), a ^{184}Ta source was used: After counting a W foil exposed to μ^- it was stripped and the residue was counted in the LLC apparatus. The resulting energy spectra are shown in Fig. 10. This procedure duplicates entirely a $\overline{\text{Mu}}$ exposure except the polarity of the beamline was μ^- rather than μ^+. After accounting for the time corrections h, the differences in Eq. (12) between a full foil and the stripped residue are the stopping fraction D and chemistry efficiency f(chemistry). The mass ratio [as in Eq. (13)] was used to estimate the relative stopping fraction D(residue) to D(foil). The resulting chemistry efficiency f(chemistry)=0.47 ± 0.03 was obtained by averaging several trials. Samples were stripped 5 to 15 times, whereas the W foil from a $\overline{\text{Mu}}$ exposure was only stripped twice.

As a check of the above value of f(chemistry), off-line tests were done using ^{187}W obtained by thermal neutron irradiation of a W foil. The isotope ^{187}W has a 24 h half-life,[36] emitting a 480 keV γ when it decays. The neutron irradiated foil was counted in the LLC apparatus, stripped several times, and the residue was counted. Since ^{187}W was uniformly distributed through the foil, the fraction of ^{187}W in the full and stripped samples is given by Eq. (13), and number of E(prompt)=480 keV γ's detected is given by Eq. (12). Averaging several trials, the chemical extraction efficiency measured by this off-line method was 0.9 ± 0.1. The large discrepancy between the ^{187}W and ^{184}Ta results might be attributable to different chemical properties of W and Ta. We used the lower value of f(chemistry)=0.47 ± 0.03 in determining our sensitivity.

G. ^{184}Ta detection efficiency

The previous two sections discussed the fraction of muonium atoms which converted to antimuonium and produced ^{184}Ta in the sample. The detection efficiency g for ^{184}Ta in the LLC apparatus is now discussed.

^{184}Ta, with an 8.7 h half-life, emits a β to excited states of ^{184}W.[36,38] The primary decay branch [with probability g(decay)=0.74 ± 0.01] has a 1.17 MeV β in coincidence with a 414 keV γ to arrive at the metastable 1.285 MeV level. The metastable state has an 8.3 μs half-life, emitting two or more γ's to arrive at the ground state. The relevant branches of the ^{184}Ta decay scheme are illustrated in Fig. 4. Figure 10 clearly shows the efficiency of the suppression of background events by demanding the full β-γ-γ_{del} signature in the LLC apparatus.

To measure $g(\gamma)$ and $g(\beta)$, a calibrated ^{198}Au source was used; ^{198}Au emits a 0.961 MeV β in coincidence with a 412 keV γ.[36] The combined photopeak efficiencies in both detectors for 412 keV γ's was $g(\gamma)$=0.074 ± 0.002. The ratio of β-γ events

to γ events with E(prompt)=412 keV from the ^{198}Au source gives a beta efficiency of $g(\beta)$=0.53 ± 0.01. As a check of $g(\beta)$, for stripped samples containing ^{184}Ta the number of β-γ-γ_{del} events was compared to the number of γ-γ_{del} events, resulting in a β efficiency of 0.50 ± 0.02, consistent with the more accurate value above.

The delayed γ efficiency of the LLC apparatus was determined using a ^{184}Ta -source. For a W foil exposed in a μ^- beam, the ratio of the number of γ-γ_{del} events with a prompt energy of 414 ± 3 keV to the number of γ events with the same energy gives the delayed γ efficiency $g(\gamma_{del})$=0.421 ± 0.003. To eliminate the γ-γ_{del} background due to the metastable ^{72}Ge state (discussed in Sec. III D), all events with delayed γ energy of 690–710 keV were rejected, with a negligible 0.3% reduction in the delayed γ efficiency.

A fraction of the delayed γ's from ^{184}Ta occurred during the integration time of the Ge detector amplifier; the probability is g(pileup) that a delayed γ during this time will shift the prompt γ energy from 414 keV. For events with both the prompt and delayed γ's in the same detector, Fig. 11 shows the time distribution of γ-γ_{del} events observed while counting a ^{184}Ta source [these events have E(prompt)=414 ± 3 keV]. Few events were observed during the first 4 μs since the prompt γ energy was shifted by the delayed γ energy, so all events were rejected when both the prompt and delayed γ were in the same detector and delay time was t(delay) < 4 μs. For events where a delayed γ was detected [with t(delay) < 4 μs] in the opposite Ge detector as the prompt γ, an additional delayed γ could shift the prompt γ energy from 414 keV. Multiplying the probability that the ^{184}W metastable state will decay during the Ge detector amplifier integration time by the fraction of delayed γ's entering the same detector as the prompt γ, the calculated probability of a delayed γ shifting the prompt γ energy is g(pileup)=0.93 ± 0.02.

V. RESULTS

In the summer 1988 run, there were 50 $\overline{\text{Mu}}$ exposures, with N_μ=(2.3 ± 0.2)×10^{12} incident μ^+ during 525 h of beam time. The total counting time in the LLC apparatus was 602 h. Figure 12 shows the prompt gamma energy for γ, γ-γ_{del}, and β-γ-γ_{del} events observed in the LLC apparatus (after applying all cuts).

Exposure 24, which was counted immediately following a μ^- exposed W foil, appeared to be contaminated with ^{184}Ta, and was excluded from the analysis. A contamination of less than 1.5 mg of the previous W sample left in the LLC apparatus would account for the four γ-γ_{del} and six β-γ events [with E(prompt)=414 ± 3 keV] observed while counting exposure 24. A total of only 26 γ-γ_{del} events with energy of E(prompt)=414 ± 3 keV were observed in all 51 exposures, so the probability of four occurring in one run is < 0.1%.

If the cut on the delayed γ energy (used to suppress the ^{72}Ge background discussed in Secs. III D and IV G) is not imposed, one candidate β-γ-γ_{del} event with E(prompt)=414 ± 3 keV survives all other cuts. The prompt γ had an energy of E(prompt)=412.9 ± 0.3 keV and a β scintillator pulse height well above the noise threshold. The delayed γ for this event had an energy of E(delay)=694 keV and occurred t(delay)=760 ns after the prompt γ. Both the delayed γ energy and time are consistent with the background due to the metastable ^{72}Ge state with 439 ns half-life and γ energy of 691 keV, thus it was eliminated by the delayed γ energy cut.

Using the values from Table I and the total number of muons, the sensitivity of the experiment was

$$S = N_\mu \epsilon_\mu = (1.1 \pm 0.2) \times 10^6. \qquad (14)$$

In Appendix B, an expression is derived for the upper limit on the number of observed

events in an experiment which has an uncertainty in sensitivity. For no observed events in this experiment with a 20% uncertainty, the 90% confidence upper limit on the number of events is 2.42, in contrast to 2.3 events in the absence of uncertainty. Therefore, the 90% confidence upper limit on $P(\overline{\text{Mu}})$ is 2.2×10^{-6}. By including the 100 h of data taken in November 1987[5] (see Appendix C) the resulting upper limit for the probability, $P(\overline{\text{Mu}})$, of muonium–antimuonium conversion is:

$$P(\overline{\text{Mu}}) < 1.9 \times 10^{-6} \quad (90\% \text{ confidence}) \tag{15}$$

corresponding to an upper limit on the effective four-fermion coupling strength of

$$G < 0.28 \ G_F \quad (90\% \text{ confidence}). \tag{16}$$

Equation (6) expresses the relationship between the Mu to $\overline{\text{Mu}}$ coupling constant G and parameters of a left-right symmetric model. Our upper limit on G constrains this model to

$$\frac{f_{ee} f_{\mu\mu}^*}{g^2} \left(\frac{M_W}{M_{++}} \right)^2 < 0.28 \quad (90\% \text{ confidence}). \tag{17}$$

Under the assumption that the couplings f_{ee} and $f_{\mu\mu}^*$ are of the same order as g, the constraint on the mass of the doubly charged boson is

$$M_{++} \gtrsim 150 \text{ GeV}/c^2. \tag{18}$$

ACKNOWLEDGMENTS

Appendix A. SURFACE CONTAMINATION STUDIES

A μ^- will transfer to tungsten atoms from a contaminant which is chemically bonded ("chemisorbed") to the surface, however if the contaminant is not chemically bound to the surface ("adsorbed"), it is not clear that a μ^- will transfer to the heavier tungsten atoms nearby. Of particular concern were carbon and H_2O contamination, since they constituted a large fraction of the residual gas in the vacuum system. A clean W surface accumulates carbon[39] when exposed to CO or CO_2, however carbon does not adsorb on oxidized W surfaces.[40] H_2O adsorbs on some oxidized surfaces but not on others,[41] with a dependence on the method of preparation of the surface. In particular, published studies of $Na_{0.7}WO_3$ (001) crystals found that H_2O adsorbs at 150K, but not at room temperature.[42] In this appendix, we describe measurements taken to quantify the fraction of the surface which was not covered by contaminants.

In Auger electron spectroscopy (AES) an electron beam strikes a sample and causes an atom to emit an Auger electron. Electrons directly from the electron beam cause most of the ionization, however some beam electrons are backscattered deep within a sample and ionize atoms near the surface. Figure 13 shows the AES spectra obtained after a W foil is cleaned in an O_2 plasma. To identify elements, high resolution scans [e.g. Fig. 14(a)] were compared with reference spectra[32] [e.g. Fig. 14(b)] displayed in a similar manner. The concentration of particular elements was determined by comparing the peak to peak heights of the spectra to reference samples.

We also compared photoelectron spectra created by x-ray photoelectron spectroscopy (XPS or electron spectroscopy for chemical analysis, ESCA) with reference spectra.[33] Shifts in photoelectron binding energies E_B can be used to determine chemical bonds of elements to other atoms. The kinetic energy of the photoelectron is the difference of the electron binding energy and the x-ray energy.

The range, in material A, of electrons with kinetic energy E (from either AES or XPS) is called the inelastic mean free path (IMFP).[43,44] Only electrons from the first few IMFP's have sufficient energy to escape from the sample to the spectrometer. For electrons of kinetic energy $E > 150$ eV, in material A with atomic size a nm, the IMFP is given by

$$\lambda^A(E) = k(aE)^{1/2} \text{ monolayers } [\pm 37\%],\qquad(A1)$$

with k values of 0.41 for elements, 0.55 for oxides, and 0.72 for other inorganic compounds. Electrons from our samples have IMFP ranges of 3 monolayers (for W Auger electrons in W) to 9 monolayers (for W photoelectrons in WO_3).

Seah and Dench[43] derive expressions for the signal due to a contaminant A adsorbed on the surface of a uniform sample. The intensity I^A of A electrons (emerging at angle θ) from a fraction X of a monolayer of adsorbate is

$$I^A = X I_\infty^A R_A (1 - f_A),\qquad(A2)$$

where the attenuation of the peak by a monolayer of adsorbate A is

$$f_A = \exp\left[\frac{-\sec\theta}{\lambda^A(E_A)}\right].\qquad(A3)$$

The ratio of the backscatter factors[45] $[r_W(E_A)$ and $r_A(E_A)$ given in Ref. 45]

$$R_A = [1 + r_W(E_A)] / [1 + r_A(E_A)]\qquad(A4)$$

accounts for the different backscattering of beam electrons from bulk samples of A and W. X rays do not backscatter, so for XPS $r_W = r_A = 0$.

For a plasma cleaned sample, the expression for W electron intensity is more complicated than in Ref. 43 since W electrons originated from both surface WO_3 and the W substrate. For a fractional monolayer X of A adsorbed, the respective signals from n monolayers of WO_3 over a W substrate are

$$I^{WO_3} = I_\infty^{WO_3} R_{WO_3} (1 - g^n) [X(f_W - 1) + 1] \qquad (A5)$$

$$I_S^W = I_\infty^W g^n [X(f_W - 1) + 1], \qquad (A6)$$

where the backscattering correction is

$$R_{WO_3} = [1 + r_W(E_W)] / [1 + r_{WO_3}(E_W)]. \qquad (A7)$$

The total intensity of W Auger electrons (or photoelectrons) is

$$I^W = I^{WO_3} + I_S^W. \qquad (A8)$$

Electron attenuation factors (for electron energy E_W) for single monolayers of A and WO_3, respectively, are

$$f_W = \exp\left[\frac{-\sec\theta}{\lambda^A(E_W)}\right] \qquad (A9)$$

$$g = \exp\left[\frac{-\sec\theta}{\lambda^{WO_3}(E_W)}\right]. \qquad (A10)$$

Solving Eqs. (A2) and (A8), the fractional coverage X by contaminant A is

$$X = \left\{ \frac{I^W}{I^A} \frac{I_\infty^A}{I_\infty^W} \frac{(1 - f_A)R_A}{Q(1 - g^n)R_{WO_3} + g^n} + 1 - f_W \right\}^{-1}, \qquad (A11)$$

where $Q = I_\infty^{WO_3}/I_\infty^W$.

The surface tests were done in a separate vacuum system at the Surface Physics Laboratory at Simon Fraser University. The UHV ($\sim 10^{-10}$ Torr) section of this vacuum system contained a PHI 255–GAR double pass cylindrical mirror analyzer (CMA) spectrometer mounted at $\theta = 45°$ to the sample. Excitation of the sample for AES and XPS was done by a 3 keV electron source and Mg $K\alpha$ x-ray source (x-ray energy 1253.6 eV) respectively. An argon gun allowed removal of surface layers by sputtering. Samples were prepared in the small "intro chamber" ($\sim 10^{-6}$ Torr) of the vacuum system, before insertion into the UHV spectrometer section.

The surface testing procedure went as follows: A tungsten foil was introduced into the spectrometer to determine initial contamination of the surface. Next, the sample was oxygen plasma cleaned (as described in Sec. III A) in the intro chamber. AES and XPS spectra were taken to study contamination immediately following the plasma cleaning. To simulate the vacuum exposure incurred during a $\overline{Mu}$ exposure (~ 2200 L, where a Langmuir is defined as 1 L $= 1 \times 10^{-6}$ Torr s), the sample was moved to the intro chamber, at 10^{-5} Torr, for a period of time. Following this vacuum exposure, the sample was re-inserted into the UHV section of the spectrometer and final spectra were taken. Comparison of spectra before and after the vacuum exposure allows determination of contamination which built up on the surface. To increase the sensitivity of the surface tests, samples had vacuum exposures in the intro chamber of between 6000 L and 1.2×10^5 L.

The amplitude of the tungsten XPS lines was used to determine the number of monolayers of WO_3 formed when the sample was plasma cleaned. Figure 15 shows the XPS spectra for $E_B=42$ to 28 eV, containing the $4f_{7/2}$ and $4f_{5/2}$ peaks from W and WO_3. The position of these peaks is in agreement with Ref. 46. Four Gaussian peaks, plus a linear background, were fitted to this region, giving respective areas under the WO_3 and W peaks of $I^{WO_3} = 3.6 \pm 0.7$ and $I_s^W = 2.4 \pm 0.6$ (arbitrary units). The ratio of the tungsten XPS signal from thick WO_3 and W samples is calculated to be $Q_{XPS} = I_\infty^W/I_\infty^{WO_3} = 0.6$ by using the respective densities of WO_3 and W, along with the differences of IMFP's in the materials. Using Eqs. (A5) and (A6), the observed areas indicate that at least seven monolayers of WO_3 are formed on the surface after plasma cleaning.

Due to differences in shape and amplitude of the tungsten AES peak from W and WO_3 samples, the sensitivity of the W Auger line from WO_3 must be determined. A WO_3 surface was evaporated onto a W substrate in the intro chamber. Since the evaporated layer was several IMFP's thick, the observed AES W line for this sample was due to WO_3. Next the WO_3 was sputtered away with the argon gun, leaving the W substrate. Comparing the peak to peak amplitude $I_\infty^{WO_3}$ of the thick WO_3 layer (after correcting for electrons backscattered from the W substrate[45]) to the amplitude I_∞^W from the W foil, the relative sensitivity was $Q_{AES} = I_\infty^{WO_3}/I_\infty^W = 0.42 \pm 0.06$ for AES. For comparison, Lin and Lichtman[47] bombarded a WO_3 powder with an intense electron beam to selectively desorb oxygen, leaving metallic W. The change in signal amplitude of their sample after this desorption gives $Q_{AES} = 0.36 \pm 0.08$ after accounting for backscattering from WO_3.

On W samples, both before and after plasma cleaning, AES lines characteristic of potassium and calcium were observed. The AES sensitivity of these elements is high, so small concentrations created large peaks. Nearly all of this contamination was on the surface, because sputtering removed most of the signal. The potassium signal was also greatly reduced by anodizing and stripping the W surface (as done for $\overline{Mu}$ exposures) before the sample was plasma cleaned. The W foils for $\overline{Mu}$ exposures were reused many times, thus K or Ca contamination on the surface would be removed. The small amounts of K and Ca observed on a stripped W foil (Fig. 14) are likely to be chemically bonded to W, so they were disregarded.

Auger electron spectroscopy is much more sensitive to carbon than tungsten, so accurate contamination studies could be performed. The AES spectra for a plasma cleaned sample is shown in Fig. 14 along with K, Ca,[32] and several chemical forms of carbon.[48] A common feature of all forms of carbon is a main minimum at ≈ 272 eV with changes in the shape depending on chemical composition. Because of the proximity of K and Ca peaks, it was not possible to use the carbon peak shape in determining the chemical composition of the carbon on the samples. The low XPS sensitivity to carbon precludes observation of the XPS carbon peak, so no information about the chemical state of the carbon was available. We used the conservative assumption that all structure observed in the AES spectra between 260 and 275 eV was due to carbon adsorbed on the surface of the sample.

Before plasma cleaning, a thick carbon layer ($\gtrsim 2$ monolayers) was observed on a W foil. After plasma cleaning, the peak to peak amplitude of the AES tungsten and carbon lines illustrated in Figs. 13 and 14(a) were $I^W = 33 \pm 2$ and $I^C = 5.4 \pm 1.1$ (arbitrary units). Using the values given in Table II, Eq. (A11) places a limit on the carbon contamination of 0.12 ± 0.03 monolayers after averaging several samples. No change was observed for vacuum exposures of over 1.2×10^5 L, many times longer than the 2200 L of a typical $\overline{Mu}$ exposure. The actual coverage of the surface by adsorbed carbon is presumably less than the above value since: (a) previous studies[40]

indicate CO does not adsorb on WO_3 surfaces, (b) the observed carbon is probably in the bulk W sample and not on the surface, (c) the carbon may be chemically bonded to the W and thus the μ^- will transfer, (d) conservative estimates were used for all parameters.

Since a major fraction of the residual gas in the vacuum system was water vapor, it was necessary to insure H_2O was not adsorbed on the surface. Figure 16 shows the XPS line for oxygen photoelectrons from a plasma cleaned W samples, along with the published spectrum for an oxidized W surface prepared in high vacuum.[49] The XPS oxygen line for H_2O adsorbed on Fe_2O_3 and oxidized Pb, Ni, and Cu is shifted at least 2 eV to higher binding energy from respective the oxide line.[41] The dotted line in Fig. 16 is a simulated XPS oxygen spectrum expected from a 15% contamination of H_2O adsorbed on the WO_3 surface. To obtain this spectra, a peak shifted by 2 eV was added to the XPS oxygen spectrum of Ref. 49. The shape of this peak was identical to the main O peak and the area of the modeled H_2O peak was determined by Eq. (A11) for the XPS O peak due to H_2O adsorbed on seven monolayers of WO_3. No evidence for H_2O on the plasma cleaned sample was seen, in agreement with Ref. 42 where water vapor adsorbed on $Na_{0.7}WO_3$ was found to be unstable at room temperature.

In conclusion, the only contaminant on the plasma cleaned WO_3 surface is carbon, with an upper limit of 0.12 ± 0.03 monolayers, thus the fraction $e(\text{surface})=0.88 \pm 0.03$ was free from contaminants.

Appendix B. UPPER LIMIT ON NUMBER OF EVENTS

In this experiment, no candidate Mu–$\overline{\text{Mu}}$ conversion events were observed. Determination of an upper limit on the number of observed events is discussed in many sources[50,51] when there is no uncertainty in the sensitivity of the experiment. To our knowledge, the approach to the problem when the sensitivity has experimental uncertainty has not been adequately discussed. In this appendix, an expression is derived for the upper limit on the number of observed events when the experimental sensitivity is uncertain. The symbol S_0 denotes the true sensitivity of the experiment, while $(S \pm \sigma_S)$ is the experimental estimate of the sensitivity S_0.

In a counting experiment, the number n of observed events has a Poisson distribution:

$$f(n; \mu) = \frac{e^{-\mu}\mu^n}{n!} \quad , \quad (n = 0, 1, 2, \cdots). \tag{B1}$$

For a process with probability P (e.g. the muonium–antimuonium conversion probability, or the branching ratio of a decay process) and experimental sensitivity S_0, the mean of the distribution is $\mu_0 = PS_0$. When n_0 events are observed and the value of P is not known, an upper limit on μ_0 is desired. In the absence of experimental uncertainty, Ref. 50 shows that the probability CL for $n > n_0$ events being observed is

$$\text{CL} = 1 - \sum_{n=0}^{n_0} f(n; N), \tag{B2}$$

where the mean N is an upper limit on the Poisson mean μ_0. Frequently in rare decay experiments, no candidate events are observed ($n_0 = 0$), thus

$$\text{CL} = 1 - e^{-N} \tag{B3}$$

which has a value of $N = 2.30$ at confidence level CL=90%. The corresponding upper limit on P at confidence CL is $P = N/S_0$.

In an experimental search, the sensitivity is $S \pm \sigma_S$, or a relative uncertainty $\eta = \sigma_S/S$. The mean $\mu = PS$ of the Poisson distribution of Eq. (B1) will have this same relative uncertainty η, and standard deviation $\sigma_\mu = \mu\eta$. Since the sensitivity is non-negative, a truncated Gaussian was used to model the distribution of μ, namely

$$\tilde{g}(\mu'; \mu, \sigma_\mu^2) = Kg(\mu'; \mu, \sigma_\mu^2) \quad , (\mu' \geq 0), \tag{B4}$$

where $g(\mu'; \mu, \sigma_\mu^2)$ is the Gaussian distribution

$$g(\mu'; \mu, \sigma_\mu^2) = \frac{1}{\sigma_\mu\sqrt{2}} \exp\left[\frac{-(\mu' - \mu)^2}{2\sigma_\mu^2}\right] \tag{B5}$$

and normalization K is given by

$$\frac{1}{K} = \int_{\mu'=0}^{\infty} g(\mu'; \mu, \sigma_\mu^2)d\mu' = \frac{1}{2}\left[1 + \text{erf}\left(\frac{\mu}{\sigma_\mu\sqrt{2}}\right)\right]. \tag{B6}$$

Since the probability of a given value of μ' is $\tilde{g}(\mu'; \mu, \sigma_\mu^2)$, it follows that the probability of observing n events from distribution of mean μ' is

$$f(n; \mu')\,\tilde{g}(\mu'; \mu, \sigma_\mu^2)\,d\mu' \quad , (n = 0, 1, 2, \cdots), \tag{B7}$$

where $f(n; \mu')$ is given by Eq. (B1). For a given confidence level CL, the corresponding upper limit N of the Poisson mean μ is obtained by solving

$$\text{CL} = 1 - \sum_{n=0}^{n_0} \int_{\mu'=0}^{\infty} \frac{e^{-\mu'}\mu'^n}{n!}\tilde{g}(\mu'; N, \sigma_\mu^2)d\mu'. \tag{B8}$$

When $n_0 = 0$ (no observed events) the confidence limit reduces to

$$\text{CL} = 1 - \int_{\mu'=0}^{\infty} e^{-\mu'}\tilde{g}(\mu'; N, \sigma_\mu^2)d\mu'. \tag{B9}$$

Integrating this expression[52] gives a confidence level

$$\text{CL} = 1 - \left\{\frac{1 + \text{erf}\left[(1 - N\eta^2)/(\eta\sqrt{2})\right]}{1 + \text{erf}\left[1/(\eta\sqrt{2})\right]}\right\} \exp\left[-N + (N\eta)^2/2\right] \tag{B10}$$

with the relative uncertainty η defined above. As expected, in the absence of error ($\eta \to 0$) the confidence level reduces to Eq. (B3).

Figure 17 is a plot of the 90% confidence upper limit on μ, obtained by numerically solving Eq. (B10) for different relative uncertainties $\eta = \sigma_S/S$. This upper limit on the number of events is insensitive to small values of η; thus $\mu = 2.3$ is a reasonably good approximation for experiments with small relative uncertainties, however it is a serious underestimate for experiments with an uncertainty greater than 20%.

For our experimental sensitivity [Eq. (14): $S = (1.15 \pm 0.22) \times 10^6$] the uncertainty is $\eta = 0.20$. The corresponding 90% confidence upper limit on the number of events (from Fig. 17) is $\mu = 2.42$, thus the upper limit on the probability that a Mu atom will convert to $\overline{\text{Mu}}$ is

$$P(\overline{\text{Mu}}) < 2.42/1.15 \times 10^6 = 2.1 \times 10^{-6} \quad (90\% \text{ confidence}). \tag{B11}$$

Appendix C. NOVEMBER 1987 RUN

An earlier run of this experiment, which took 100 h of data $[N_\mu = (4.0 \pm 0.2) \times 10^{11}]$, resulted in a published upper limit[5] of $G < 0.88\ G_F$. Because of changes in the technique and apparatus, and more detailed measurements, the values of some factors in this earlier run (November 1987) are different than the values in Sec. IV and in Ref. 5. The differences in the two runs are discussed below; unless otherwise noted, all efficiencies are the same as values in Table I.

The catcher in the November 1987 run was a flat W foil on which WO_3 was evaporated. The absence of wings leads to the smaller values of e(catcher)=0.147 ± 0.005 and e(recoil)=0.49 ± 0.01.

The surface tests on the evaporated WO_3 surface indicate an upper limit of e(surface)=0.9. This is due to a smaller observed C line in AES, probably indicating the carbon observed for plasma cleaned samples is in the bulk of the W sample.

The chemistry efficiency f(chemistry) for the November 1987 run was different than for the summer 1988 run. The evaporated WO_3 layer was dissolved in NH_4OH before the surface was anodized. A ^{184}Ta recovery of > 90% was measured under these conditions. The range of 33 keV ^{184}Ta in amorphous WO_3 is much less than W,[28] thus most of the ^{184}Ta will stay in the evaporated layer. An additional 60 nm of the W substrate was anodized and removed, with a recovery efficiency of 0.47 ± 0.02 as discussed in Sec. IV F. We estimate the chemistry efficiency for this run to be f(chemistry)=0.8 ± 0.15.

In the summer 1988 run, a larger, lower background Ge detector replaced one of the Ge detectors previously used. The appropriate g values for the 1987 run are $g(\gamma)$=0.052 ± 0.001, $g(\beta)$=0.55 ± 0.01, and $g(\gamma_{del})$=0.34 ± 0.02. A 7 μs integration time was used for the Ge detectors, so the pileup factor was g(pileup)=0.85 ± 0.01.

A total of 11 $\overline{Mu}$ exposures occurred during this run, and several of the exposures were counted for over a day. The resulting time correction for these exposures was 0.68 ± 0.01.

REFERENCES

* Present address: Gusta··us Adolphus College, St. Peter, Minnesota 56082.
* Present address: National Laboratory for High Energy Physics (KEK), Ibaraki
-305, Japan.
† Present address: Carleton University, Ottawa, Ontario, Canada K1A 0R6.
‡ Present address: TRIUMF, Vancouver, British Columbia, Canada V6T 2A3.

[1] S. L. Glashow, Nucl. Phys. **22**, 579 (1961); S. Weinberg, Phys. Rev. Lett. **19**, 1264 (1967); A. Salam, in *Elementary Particle Theory: Relativistic Groups and Analyticity (Nobel Symposium No. 8)*, edited by N. Svartholm (Almqvist and Wiksell, Stockholm, 1968), p. 367.

[2] J. J. Amato *et al.*, Phys. Rev. Lett. **21**, 1709 (1968).

[3] W. C. Barber *et al.*, Phys. Rev. Lett. **22**, 902 (1969); G. M. Marshall *et al.*, Phys. Rev. D **25**, 1174 (1982); B. Ni *et al.*, Phys. Rev. Lett. **59**, 2716 (1987); Nuc. Phys. **A478**, 757c (1988).

[4] G. A. Beer *et al.*, Phys. Rev. Lett. **57**, 671 (1986).

[5] T. M. Huber *et al.*, Phys. Rev. Lett. **61**, 2189 (1988).

[6] H. J. Mundinger *et al.*, Proceedings Rare Decay Symposium, Vancouver, 1988 (World Scientific, Singapore, in press).

[7] K. Nishijima, Phys. Rev. **108**, 907 (1957); J. Schwinger, Ann. Phys. **2**, 407 (1957).

[8] G. Feinberg and S. Weinberg, Phys. Rev. Lett. **6**, 381 (1961); a multiplicative law which includes the τ generation is discussed by E. Derman, Phys. Rev. D **19** 317 (1979).

[9] F. Bergsma *et al.*, Phys. Lett. **122B**, 465 (1983); S. E. Willis *et al.*, Phys. Rev. Lett. **44**, 522 (1980); **45**, 1370(E) (1980).

[10] B. Pontecorvo, Zh. Eksp. Teor. Fiz. **33**, 549 (1957); translation, Sov. Phys. JETP **6**, 429 (1958).

[11] G. Feinberg and S. Weinberg, Phys. Rev. **123**, 1439 (1961).

[12] R. N. Mohapatra and G. Senjanović, Phys. Rev. Lett. **44**, 912 (1980); Phys. Rev. D **23**, 165 (1981).

[13] E. Witten, Phys. Lett. **91B**, 81 (1980).

[14] M. Gell-Mann, P. Ramond and R. Slansky, in *Supergravity*, editors P. van Nieuwenhuizen and D. Freedman (North-Holland, Amsterdam, 1980); T. Yanagida, in *Proc. Workshop on Unified Theory and Baryon Number in the Universe*, editors O. Sawada and A. Sugamoto, (KEK 1979); H. Harari and Y. Nir, Nucl. Phys. **B292**, 251 (1987).

[15] A. Halprin, Phys. Rev. Lett., **48**, 1313 (1982).

[16]G. K. Leontaris, K. Tamvakis, and J. D. Vergados, Phys. Lett. **162B**, 153 (1985).

[17]P. Herczeg, Proceedings Rare Decay Symposium, Vancouver, 1988 (World Scientific, Singapore, in press); P. Herczeg and R. N. Mohapatra, in preparation.

[18]C. E. Picciotto and M. S. Zahir, Phys. Rev. D **26**, 2320 (1982).

[19]W. C. Haxton, S. P. Rosen, and G. J. Stephenson, Jr., Phys. Rev. D **26**, 1805 (1982).

[20]G. B. Gelmini and M. Roncadelli, Phys. Lett. **99B**, 411 (1981).

[21]V. Barger, W. Y. Keung, and S. Pakvasa, Phys. Rev. D **25**, 907 (1982); V. Barger, H. Baer, W. Y. Keung, and R. J. N. Phillips, Phys. Rev. D **26**, 218 (1982); C. E. Picciotto et al., Phys. Rev. D **37**, 1131 (1988).

[22]J. D. Vergados, Phys. Rep. **133**, 1 (1986).

[23]G. K. Leontaris, K. Tamvakis, and J. D. Vergados, Phys. Lett. B **171**, 412 (1986); V. Bhansali and H. Georgi, Phys. Lett. B **197**, 553 (1987).

[24]E. L. Mathie, *TRIUMF Users' Handbook*, 1987.

[25]*Cab-O-Sil Properties and Functions*, Technical report available from Cabot Corporation, 125 High Street, Boston, MA 02110, USA.

[26]A. C. Janissen et al., in preparation.

[27]L. Holland, Vacuum **26**, 97 (1976).

[28]M. McCargo, J. A. Davies, and F. Brown, Can. J. Phys. **41**, 1231 (1963).

[29]C. R. Westerfeldt et al., Nucl. Instrum. Methods **192**, 273 (1982); E. Eichler, P. H. Stelson and J. K. Dickens, Nucl. Phys. **A120**, 622 (1968).

[30]G. M. Marshall et al., Phys. Lett. **65A**, 351 (1978); K. A. Woodle et al., Z. Phys. D **9**, 59 (1988).

[31]D. L. Morgan, Ph.D. thesis, Yale University, 1966.

[32]L. E. Davis et al., *Handbook of Auger Electron Spectroscopy*, 2nd ed. (Physical Electronics Inc., Minnesota, 1976).

[33]C. D. Wagner et al., *Handbook of X-Ray Photoelectron Spectroscopy*, (Perkin Elmer Corp., Minnesota, 1979).

[34]T. von Egidy et al., Phys. Rev. A **23**, 427 (1981), S. Stanislaus, F. Entezami, and D. F. Measday, Nucl. Phys. **A475**, 642 (1987).

[35]T. Suzuki, D. F. Measday, and J. P. Roalsvig, Phys. Rev. C **35**, 2212 (1987).

[36]C. M. Lederer and V. S. Shirley, editors, *Table of Isotopes*, 7th ed. (Wiley, New York, 1978).

[37]B. MacDonald *et al.*, Phys. Rev. **139**, B1253 (1965).

[38]M. J. Martin and P. H. Stelson, Nucl. Data Sheets **21**, 1 (1977).

[39]R. Gomer, Jpn. J. Appl. Phys., Suppl. 2, Pt. 2, 213 (1974).

[40]C. G. Goymour and D. A. King, Surf. Sci. **35**, 246 (1973).

[41]P. A. Thiel and T. E. Madey, Surf. Sci. Rep. **7**, 211 (1987); A. Spitzer and H. Lüth, Surf. Sci. **160**, 353 (1985); C. Benndorf, C. Nöbl and F. Thieme, Surf. Sci. **121**, 249 (1983); J. H. Linn and W. E. Swartz, Jr., Appl. of Surf. Sci. **20**, 154 (1984).

[42]D. G. Aitken *et al.*, Vacuum **33**, 753 (1983).

[43]M. P. Seah and W. A. Dench, Surf. Interface Anal. **1**, 2 (1979).

[44]M. P. Seah, Surf. Interface Anal. **9**, 85 (1986).

[45]S. Ichimura and R. Shimizu, Surf. Sci. **112**, 386 (1981).

[46]R. J. Colton and J. W. Rabalais, Inorg. Chem. **15**, 236 (1976).

[47]T. T. Lin and D. Lichtman, J. Appl. Phys. **50**, 1298 (1979).

[48]S. Craig, G. L. Harding and R. Payling, Surf. Sci. **124**, 591 (1983).

[49]J. T. Yates, Jr., T. E. Madey, and N. E. Erickson, Surf. Sci. **43**, 257 (1974).

[50]Particle Data Group, Phys. Lett. B **204**, 1 (1988).

[51]W. T. Eadie *et al.*, *Statistical Methods in Experimental Physics*, (North–Holland, Amsterdam, 1971).

[52]I. S. Gradshteyn and I. M. Ryzhik, edited by A. Jeffrey, *Table of Integrals, Series and Products*, (Academic Press, New York, 1980).

Table I: Factors determining sensitivity of muonium to antimuonium search.

Symbol	Description	Value
Y	Muonium yield	0.024 ± 0.003
e(field)	Magnetic fields	> 0.98
e(catcher)	Conversion correction	0.187 ± 0.005
e(surface)	Surface contamination	0.88 ± 0.03
e(recoil)	Recoil of ^{184}W	0.57 ± 0.02
Product of e factors		0.092 ± 0.005
f(capture)	Atomic capture on W	0.67 ± 0.03
f(nuclear)	Nuclear capture	0.97 ± 0.02
f(184)	^{184}Ta production	0.107 ± 0.003
f(chemistry)	^{184}Ta recovery	0.47 ± 0.03
Product of f factors		0.032 ± 0.003
g(decay)	^{184}Ta branching ratio	0.74 ± 0.01
$g(\beta)$	β efficiency	0.53 ± 0.01
$g(\gamma)$	γ efficiency	0.074 ± 0.002
$g(\gamma_{del})$	Delayed γ efficiency	0.421 ± 0.003
g(pileup)	Loss from pileup	0.93 ± 0.02
Product of g factors		0.011 ± 0.001
h	^{184}Ta decay correction	0.56 ± 0.02
Sensitivity per Muon (ϵ_μ)		$(4.8 \pm 0.8) \times 10^{-7}$

Table II: Parameters used in estimating carbon contamination on plasma cleaned W surface.

Symbol	Description	Value
I_∞^C	C reference sample intensity	2.40 ± 0.03[a]
I_∞^W	W reference sample intensity	1.44 ± 0.04[a]
$r_W(E_C)$	W backscatter factor	0.96 ± 0.10[b]
$r_C(E_C)$	C backscatter factor	0.32 ± 0.07[b]
$\lambda^C(E_C)$	IMFP: C electron in W	3.1 ± 1.0[c]
$\lambda^C(E_W)$	IMFP: W electron in W	3.4 ± 1.1[c]
$\lambda^{WO_3}(E_W)$	IMFP: W electron in WO_3	3.6 ± 1.2[d]

[a] Reference 32.
[b] Reference 45.
[c] Reference 43.
[d] Reference 44.

FIGURES

FIG. 1. Rare decays mediated by doubly charged Higgs boson: (a) Muonium–antimuonium conversion, (b) neutrinoless double beta decay.

FIG. 2. Schematic diagram of the $\overline{\text{Mu}}$ exposure apparatus attached to the muon beamline.

FIG. 3. Schematic diagram of the low level counting (LLC) apparatus. The two halves are shown separated; when a sample was counted the apparatus was closed so the shielding touched at the dashed lines.

FIG. 4. Detail of the ^{184}Ta decay scheme. The ^{184}Ta signature in the low level counting apparatus was a β in coincidence with a 414 keV γ, with an additional delayed γ.

FIG. 5. Detail of the target area showing the SiO_2 muonium production target, catcher support (holding the W foil), and catcher rod.

FIG. 6. Detail of the catcher support showing the inserted foil.

FIG. 7. Pulse height spectrum of the beam scintillator during a μ^+ run. The peak below channel 150 is due to positron contamination of the incident beam.

FIG. 8. For all $\overline{\text{Mu}}$ exposures: delayed gamma energy, showing ^{72}Ge background at 690–710 keV.

FIG. 9. For all $\overline{\text{Mu}}$ exposures: time of delayed γ events where the delayed gamma energy is 690–710 keV. An exponential decay curve with ^{72}Ge halflife of 439 ns is superimposed on the data.

FIG. 10. For the ^{184}Ta obtained after stripping a W foil exposed to μ^-: prompt γ energy spectra observed in the LLC apparatus for (a) all events, (b) events with delayed γ, (c) events with prompt β and delayed γ.

FIG. 11. For a ^{184}Ta sample: time of delayed γ in same detector as prompt γ of energy 414 keV. Note the pileup suppression of events during the 4 μs Ge detector integration time

FIG. 12. For all $\overline{\text{Mu}}$ exposures: prompt γ energy spectra observed in the LLC apparatus for (a) all events, (b) events with delayed γ, (c) events with prompt β and delayed γ.

FIG. 13. Auger electron spectrum of a plasma cleaned W sample.

FIG. 14. Auger electron spectra in the region from 230 to 330 eV: (a) plasma cleaned W sample, (b) reference samples: C, CO and W_2C (from Ref. 48) K and Ca samples with amplitudes divided by factor of 2 (from Ref. 32). Spectra in (b) are to scale, with offsets added for clarity.

FIG. 15. X-ray photoelectron spectrum of a plasma cleaned W sample showing the 4f peaks of W and WO_3. The relative intensity of these peaks indicate at least seven monolayers of WO_3 cover the W surface after oxygen plasma cleaning.

FIG. 16. X-ray photoelectron oxygen spectra: filled dots are measured spectrum for plasma cleaned W sample, solid line is published WO_3 spectrum from Ref. 49, dashed line is simulated curve for a 15% contamination of H_2O on the WO_3 surface.

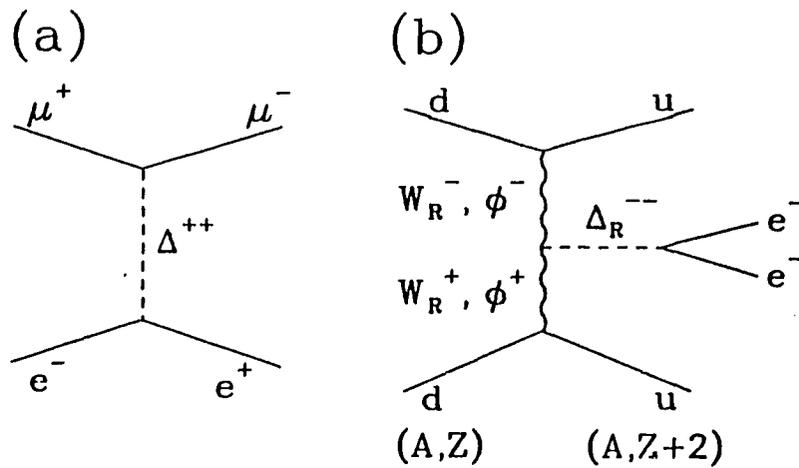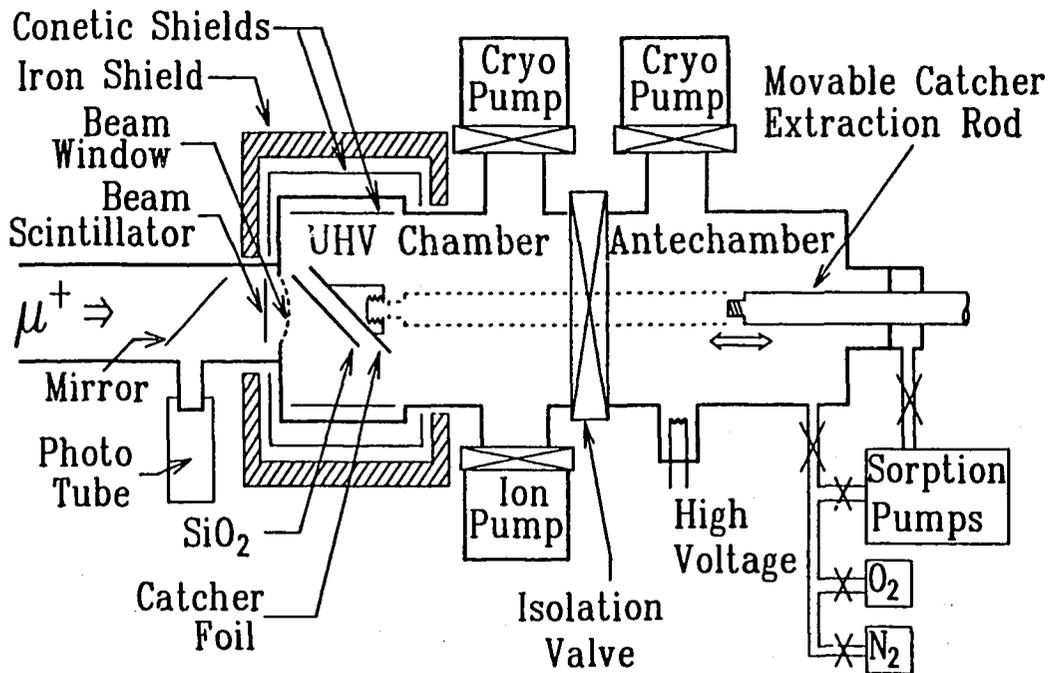FIG. 17. 90% confidence upper limit on the Poisson mean μ for relative experimental uncertainty η.
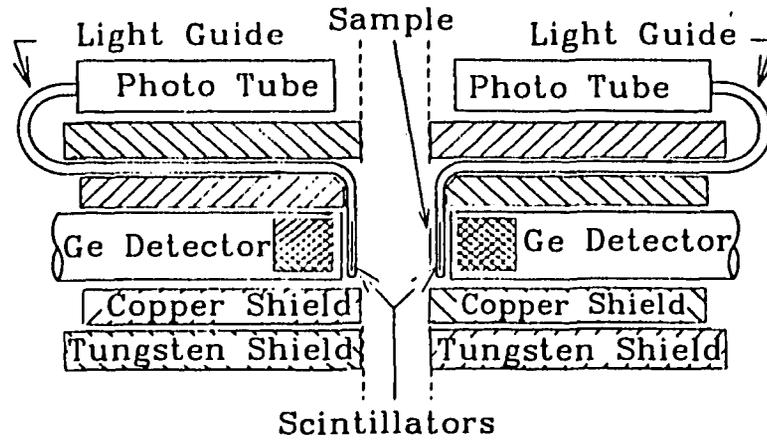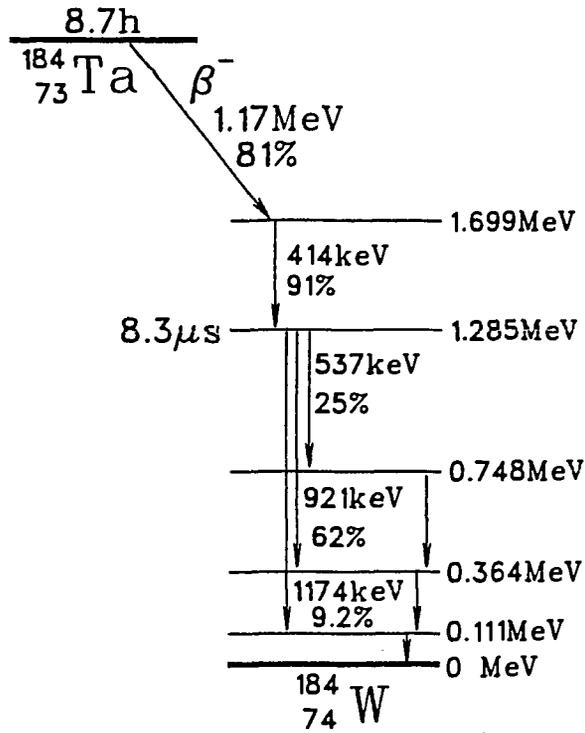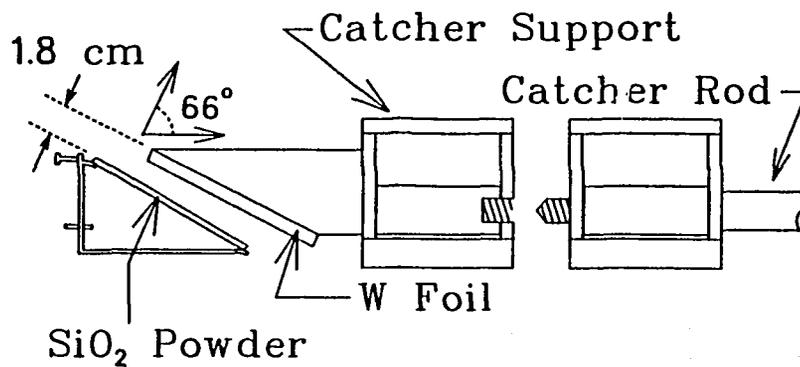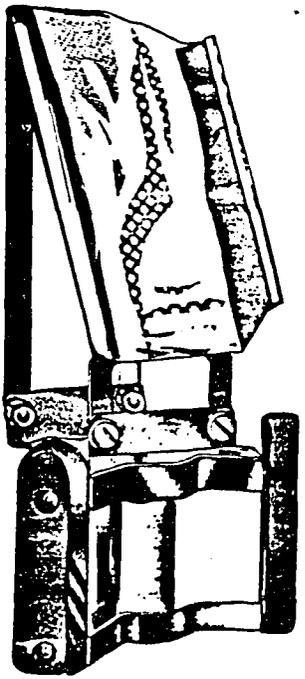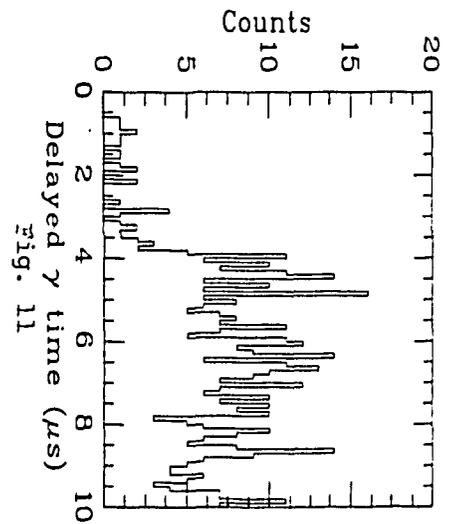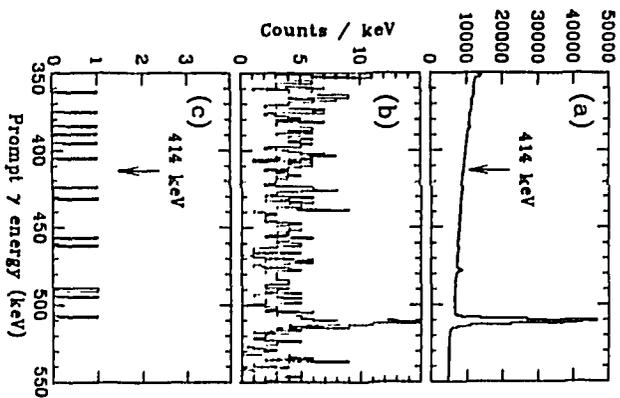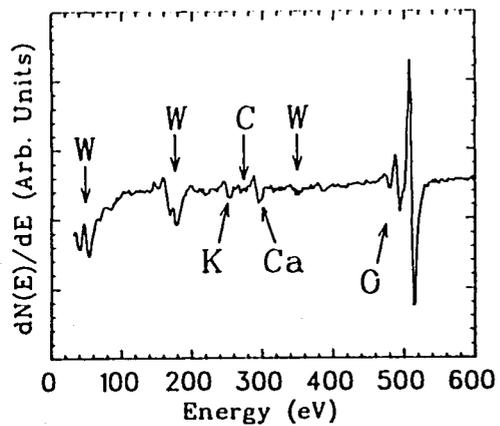

Fig. 1

Fig. 2

Fig. 3

Fig. 4

Fig. 5

Fig. 6

Fig. 7

Counts

300
250
200
150
100
50
0

Channel number
250 500 750 1000 1250

Fig. 8

Counts

150
100
50
0

691 keV

Delayed γ energy (keV)
0 200 400 600 800 1000

Fig. 9

Counts

35
30
25
20
15
10
5
0

Delayed γ time (μs)
0 1 2 3 4

Fig. 10

Counts / keV

(a) 414 keV
300
250
200
150
100
50
0

(b)
15
10
5
0

(c)
10
8
6
4
2
0

Prompt γ energy (keV)
350 400 450 500 550

Fig. 11

Counts

20
15
10
5
0

Delayed γ time (μs)
0 2 4 6 8 10

Fig. 12

Counts / keV

(a) 414 keV
50000
40000
30000
20000
10000
0

(b)
10
5
0

(c) 414 keV
3
2
1

Prompt γ energy (keV)
350 400 450 500 550

Fig. 13

Fig. 15

Fig. 17

Fig. 14

Fig. 16